PHILOSOPHICAL TRANSACTIONS OF THE ROYAL SOCIETY A MATHEMATICAL, PHYSICAL & ENGINEERING SCIENCES

High-Resolution Studies of C$_{60}$ Films by Scanning Tunnelling Microscopy

A. V. Narlikar, S. B. Samanta and P. K. Dutta

Phil. Trans. R. Soc. Lond. A 1994 **346**, 307-320
doi: 10.1098/rsta.1994.0023

High-resolution studies of C_{60} films by scanning tunnelling microscopy

By A. V. Narlikar, S. B. Samanta and P. K. Dutta
National Physical Laboratory, Dr K. S. Krishnan Road, New Delhi-12, India

Scanning tunnelling microscopic studies of C_{60} films containing conducting islands, under ambient conditions, have revealed the characteristic FCC lattice of the C_{60} clusters with intermolecular distances in various planes along different crystallographic directions closely matching with the diffraction data. The diameter of the cluster is close to 0.71 nm, i.e. the value given by the positions of the carbon atoms on the C_{60} shell, and not influenced by their π-electron lobes. The studies have revealed the nanometric defect structures in the C_{60} lattice which are found consistent with the FCC structure. The cage morphology of the buckyballs in the form of hexagons and pentagons forming the well-known icosahedral structure of the C_{60} molecule has been resolved in the finest details with bond lengths in a fair accord with the reported data. The resolved structure forming the lattice shows an orientational disorder which has been frozen from a state in which each molecule at the ambient temperature is undergoing a rotational motion which is uncorrelated with the motion of its neighbour, in conformity with diffraction and NMR results. Various possible causes of retardation and freezing of the rotational diffusion, relevant to the samples studied are discussed which also include the distortions in the carbon cages detected in the present study.

1. Introduction

The remarkable discovery of fullerenes as a third form of carbon by Kroto *et al.* (1985) and the exciting observation of superconductivity at appreciable temperatures in C_{60} solids doped with alkali metals (Hebard *et al.* 1991) have spurred a wide spread interest in the chemical, electronic and physical properties of these novel materials. Due to the breakthrough in the production technique for synthesizing them in large quantities (Kratschmer *et al.* 1990) these materials have become available in abundance for a variety of spectroscopic and diffraction studies (Bethune *et al.* 1990; Tycko *et al.* 1990*a*; Hawkins *et al.* 1991). The results obtained have corroborated the truncated icosahedral structure (soccer ball) of the C_{60} carbon cluster (CC) cage of the buckyball in the form of 12 five-member (pentagon) and 20 six-member (hexagon) rings, as originally proposed by Kroto *et al.* (1985). The atomic morphology of such a cage has also been beautifully reproduced by computer simulation (Suzuki *et al.* 1991). Lately, several attempts have been made to investigate both the molecular lattice structure as well as the atomic morphology of the carbon cage by using scanning tunnelling microscopy (STM) (Lang *et al.* 1992; Wragg *et al.* 1990; Wilson *et al.* 1990; Lamb *et al.* 1992) and atomic force microscopy (AFM) (Dietz *et al.* 1992) techniques and, indeed, the versatility and the extraordinary potential of the former in resolving the submolecular features of the cage in the finest details have been well demonstrated in the recent note by the present authors (Narlikar *et al.* 1992).

Phil Trans. R. Soc. Lond. A (1994) **346**, 307–320
Printed in Great Britain

A host of X-ray and neutron diffraction data (Hainey *et al.* 1991; David *et al.* 1991) of crystalline C_{60} have shown that at ambient temperature the molecules are orientationally disordered and the crystal structure may be described as an FCC configuration of C_{60} spheres. When the system is undoped, below 249K the molecules become orientationally ordered with a change in crystallographic symmetry from FCC to primitive (P) cubic. The low-temperature neutron diffraction data show (David *et al.* 1991) that the ensuing ordering scheme is one involving a rotational alignment of the buckyballs, such that electron-rich short inter-pentagon bonds face the electron-deficient pentagon centres of the neighbouring C_{60} cages. The NMR experiments of ^{13}C (Tycko *et al.* 1991*a*) correlate the ambient temperature disorder to the observed rapid reorientational motion of individual molecules and, at a lower temperature corresponding to the orientational order, the rotational diffusion gets significantly slowed down. The molecules execute jumps between symmetry-equivalent orientations which presumably show up as rotational alignment, as canonical snapshots, in the diffraction data (Hainey *et al.* 1991).

The STM technique is now being used extensively as a versatile tool to probe the surface morphology on the nanometric scale. This has yielded valuable information about different types of defect structures, such as interstitial atoms, dislocations, twin boundaries, growth spirals, etc., in bulk and thin-film samples of different materials having immediate relevance to their physical and chemical properties. However, there are two obvious drawbacks in the use of STM for investigating pure C_{60} samples. Firstly, their poor conductivity, with a band gap of about 1.5 eV, precludes the setting up of any measurable tunnelling currents needed for imaging. Secondly, the aforesaid rotational diffusion of the individual molecules is believed to smear out the microscopic details of the carbon cage morphology, although this need not seriously impair the imaging of the lattice framework. Interestingly, however, both these problems are circumvented in the case of samples synthesized by the variable-pressure graphite arc method. The presence of higher fullerene derivatives C_h in these samples can lower the effective energy gap due to hybridization of the electronic bands of the constituent clusters. This would make charge transfer possible, resulting in the formation of conducting islands where the STM observations become feasible (Grigoryan *et al.* 1992*a*). Also, the presence of C_h in the vicinity of C_{60}, as pointed out earlier (Dietz *et al.* 1992; Vaughan *et al.* 1991), can significantly retard or freeze the rotational diffusion, making the individual carbon cage structures visible on the nanometric scale in STM observations.

In this paper we report the results of STM studies of C_{60} films prepared by the graphite arc deposition technique. The resolved images of the molecular lattice have been related to the prominent crystallographic planes of the C_{60} structure and the presence of lattice defects has been identified. The carbon cage of the individual buckyballs has been resolved in the finest details and attempt is made to observe the assemblage of such resolved cages forming the C_{60} lattice.

2. Experimental

The samples were prepared by Grigoryan *et al.* (1992*b*) at the Indian Institute of Technology at Kanpur by using the variable-pressure graphite-arc deposition technique (Kratschmer *et al.* 1990) under the inert atmosphere of helium or argon and using graphite of spectroscopic purity. The details of the preparation are given elsewhere (Grigoryan *et al.* 1992*b*). The main difference between this technique and

PHILOSOPHICAL TRANSACTIONS OF THE ROYAL SOCIETY A MATHEMATICAL, PHYSICAL & ENGINEERING SCIENCES

that reported in Kratschmer *et al.* (1990) was that the deposition was intentionally carried out under different inert gas pressures for successive gas discharges whose time duration and numbers were also varied. These conditions are expected to vary the plasma arc temperature, typically between 8000 and 3000 K. It has been observed that by varying the growth conditions (Grigoryan *et al.* 1992*b*; Maniwa *et al.* 1991) the composition of clusters, namely C_{60}/C_h, can be suitably controlled and in the present case, the pertinent process parameters were the gas pressure, duration and the number of discharges. Carbon soot several micrometres thick was deposited over silver electrodes on a glass substrate. The characterization of these samples with XRD, SEM, electron diffraction (Grigoryan *et al.* 1992*b*) and Raman spectroscopy (Grigoryan *et al.* 1992*a*, *c*) has been described elsewhere.

In the present study, the samples were mounted on the STM (Nanoscope-II) operating at ambient conditions and the imaging was performed with mechanically sharpened Pt–Ir tips, in the constant current mode, with zero input filter and using a moderate feedback gain, as provided in the software and the scan rate was kept in the slow mode. The tips were frequently changed to avoid any artefacts.

3. Results and discussion

Owing to their high overall resistivity and inhomogeneous nature, the operation of engaging the tip to the samples and to establish and sustain the required constant tunnelling current for imaging was a paramount problem in the STM study of the deposited films. However, with repeated attempts the regions were found where the local resistivity was presumably low enough to achieve the optimum tunnelling conditions for molecular level resolution.

Figure 1*a* shows a real-time grey scale STM image in three-dimensional perspective at 60° pitch over a scan area of 15 nm × 15 nm showing the CC lattice. As may be seen, the central portion of the image appears distorted while the outer periphery exhibits a nearly square lattice pattern. Interestingly, the pertinent regions when zoomed down to a lower scan size of 7 nm × 7 nm and examined using the illumination mode software, revealed the former showing up as a triangular (or hexagonal) pattern while the latter as a square one (figure 1*b*). A closer study of the square lattice (of figure 1*a* as well of figures to follow), in the FCC configuration, corroborates the lattice parameter of about 1.4 nm of the C_{60} lattice, with the diameter of each carbon cluster agreeing with the value of 0.7 nm (Raghavachari & Rohlfing 1991). Higher CCs, for example of C_{70}, on the other hand, are known to form a hexagonal lattice (Hainey *et al.* 1991; David *et al.* 1991; Raghavachari & Rohlfing 1991), and our above observation gives credence to the simultaneous presence of both C_{60} and C_{70} clusters. Interestingly, very similar observations have been reported recently by Dietz *et al.* (1992) using AFM technique. This apart, we could resolve local regions on the nanometric scale where one set of lattice sites, namely the corner lattice points, comprised smaller size clusters (i.e. of C_{60}) while the face centring ones were distinctly larger (i.e. of C_{70}), and vice versa (figure 1*c*), indicating formation of an ordered structure of C_{60} and C_{70}. This is depicted in the image of figure 1*c* of the scan size of 3.2 × 3.2 nm in 3D perspective at 60° pitch. The fact that the STM images are obtained for these samples is itself indicative of the imaged areas being electrically conducting. This is corroborated by scanning tunnelling spectroscopic (STS) studies. The STS was performed simultaneously by first resolving the images as obtained above and subsequently by breaking up the feedback loop system at a

PHILOSOPHICAL TRANSACTIONS OF THE ROYAL SOCIETY A MATHEMATICAL, PHYSICAL & ENGINEERING SCIENCES

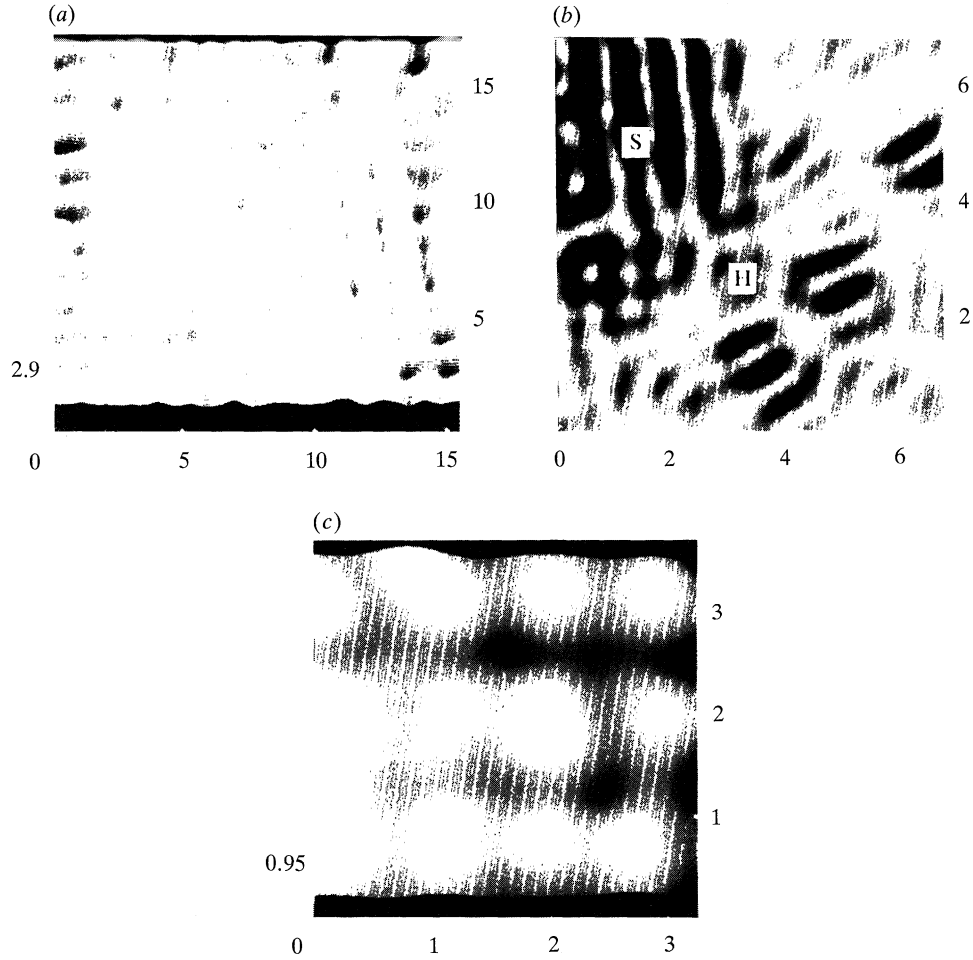

Figure 1. (*a*) Lattice-resolved CCs image in 3D perspective at 60° pitch over a scan area of 15×15 nm (bias voltage is 2400 mV and current is 50 pA; unfiltered), showing a square lattice arrangement at the outer periphery and unresolved pattern at the centre. (*b*) Zoomed image (scan size: 7×7 nm) of (*a*) covering parts the square lattice and unresolved patterns of (*a*), in the top view illumination mode revealing the unresolved pattern to be hexagonal (H) along with the square (S) lattice pattern. (*c*) Zoomed image (scan size: 3.2×3.2 nm; bias voltage is -2885 mV and current is 50 pA; moderately filtered) showing both smaller and larger size CCs on face corners and face centres of the FCC lattice.

particular instance and then switching over to the STS mode through the software. The normalized conductance spectra of $\mathrm{d}I/\mathrm{d}V$ were recorded in place of the usual $\mathrm{d}I/\mathrm{d}V$ spectra, against the bias voltage, as it eliminates any transmission factor involved between the tip and the sample surface. The normalized conductance is directly related to the local density of states (LDOS) and the spectra so obtained can reveal some insight into the electronic structure of the surface layer. The separation of the minimum of the curve at $V = 0$ from the base line is a qualitative measure of the density of states at the Fermi level E while the separation of the two branches of the curve on the positive and negative sides, where they exhibit a noticeable change in slope, gives the energy gap between the valence and conduction bands. Figure 2*a*, *b* shows the conductance spectra with drastically reduced (0.3 eV or even

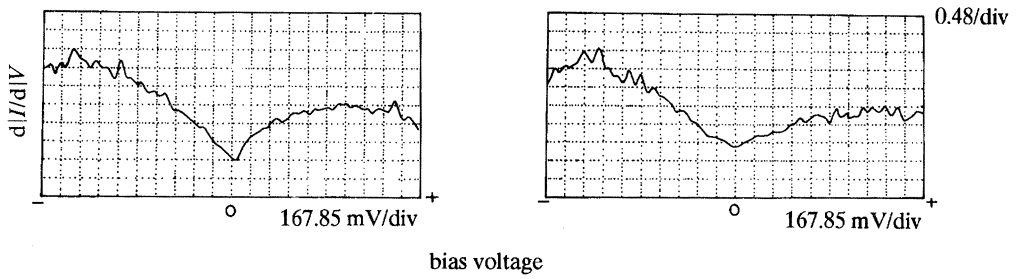

Figure 2. (*a*) Normalized conductance spectra (dI/dV) versus scanning bias voltage for the image of figure 1*a* showing the presence of a small energy gap. (*b*) Normalized conductance spectra of a different region of figure 1*a* showing a quasi-metallic energy band structure with no visible energy gap.

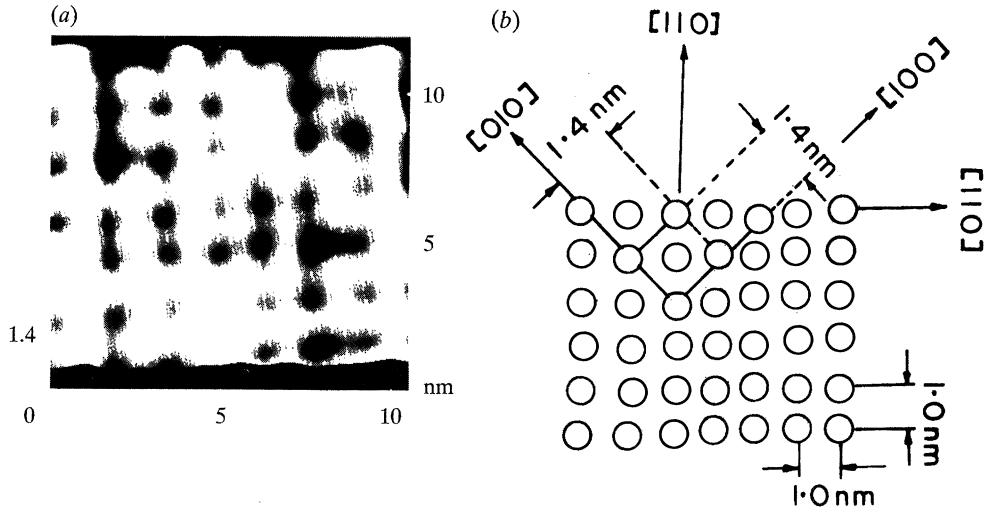

Figure 3. (*a*) Typical square lattice arrangement of CCs with no obvious lattice defects on a scan size: 10×10 nm; 3D perspective image in 60° pitch (bias voltage is -1955 mV, current is 50 pA, moderate filtering). (*b*) The sketch of the resolved pattern of (*a*) showing a square lattice pattern and the top view of FCC unit cell (001) plane. The prominent directions and intercluster distances indicated.

zero) energy gap which we attribute in part to the presence of higher carbon cluster derivatives, C_{70}, revealed in the STM studies as well as to the local distortions and defects in the carbon cage clusters which are expected to drastically lower the gap between the highest occupied molecular orbital (HOMO) and the lowest unoccupied molecular orbital (LUMO) states as theoretically predicted recently by Yi & Bernholc (1992).

In contrast to figure 1*a*, *c*, the image of figure 3*a* shows a zoomed portion of a more regular square lattice formed over a scan area of about 10 nm × 10 nm, presented in 3D perspective at 60° pitch. As may be seen from the illustrated sketch of figure 3*b*, the distances between lattice points along the prominent directions can be ideally fitted with respect to {001} planes of the C_{60} FCC lattice (Hainey *et al.* 1991; David *et al.* 1991), although some larger clusters are also seen in the lattice. The top view of one of the FCC unit cells is drawn for clarity. In accordance with the C_{60} lattice, the clusters are spaced 1 nm apart along two orthogonal ⟨110⟩ directions while their

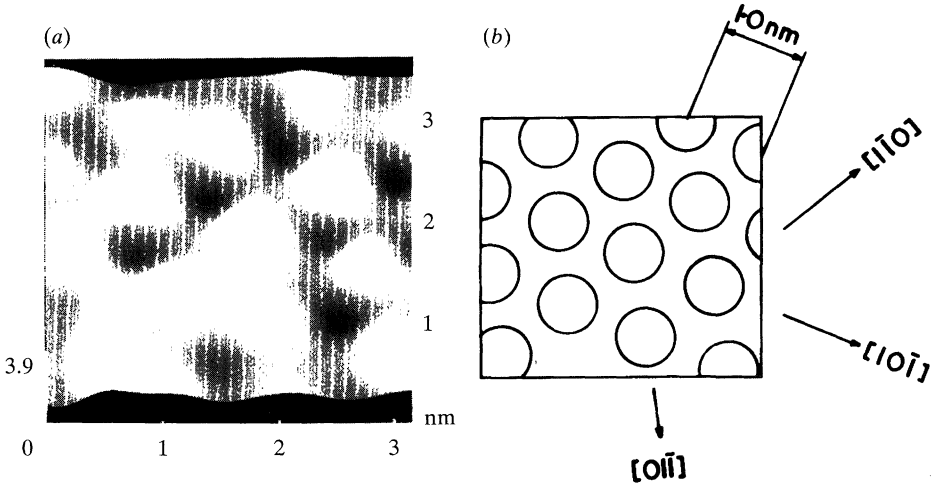

Figure 4. (*a*) Typical triangular lattice arrangement of densely packed (111) planes of FCC structure in the zoomed image over a scan area of about 3.2×3.2 nm, in 3D perspective at 60° pitch (bias voltage is -1400 mV, current is 50 pA). The diameter of the balls is 0.7 nm. (*b*) The sketch of the resolved pattern of figure 3*b* with prominent directions and distances in (111) plane indicated.

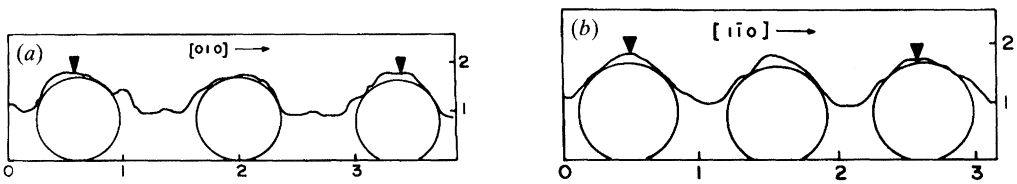

Figure 5. Section mode plots in (*a*) [010] and (*b*) [1$\bar{1}$0] directions.

separation along two orthogonal ⟨100⟩ directions is close to 1.4 nm. Similarly, in a different region of the sample, a typical lattice pattern, characteristic {111} planes in FCC structure, observed over a small area zoomed scan (size about 3 nm × 3 nm) is shown in 3D perspective at 60° pitch in figure 4*a* while figure 4*b* represents its illustrated sketch. In figure 4*a*, almost spherical 0.7 nm clusters are seen to be placed 1.0 nm apart along three ⟨110⟩ directions, forming equilateral triangles in (111) plane. The above value of the buckyball diameter and the separation distances between the neighbouring buckyballs in [010] and [1$\bar{1}$0] directions may be readily seen in the section mode plots of figure 5*a*, *b*.

It is worth noting that our value of the cage diameter is close to the one reported in the STM studies of Lang *et al.* (1992) and is smaller than the value of 1.0 nm mentioned by Wragg *et al.* (1990). The larger value is ascribed to the protruding π-electron lobes of the carbon atoms forming the C_{60} cluster and may well be attributed to a rather large tunnelling current of 1.0 nA used by these authors, which tend to make the submolecular details obscure in the STM observations. Since the present observations reveal the cage diameter to be closer to 0.71 nm, i.e. the value which is given by the positions of the carbon atoms (Raghavachari & Rohlfing 1991), it suggests that the system is perhaps better described in terms of π-molecular orbitals rather than π-valence orbitals (Douglas & McDaniel 1965). Moreover, it is known that the lobes tend to get flattened when the system turns more conducting or with the application of the electric field which should make the underlying submolecular

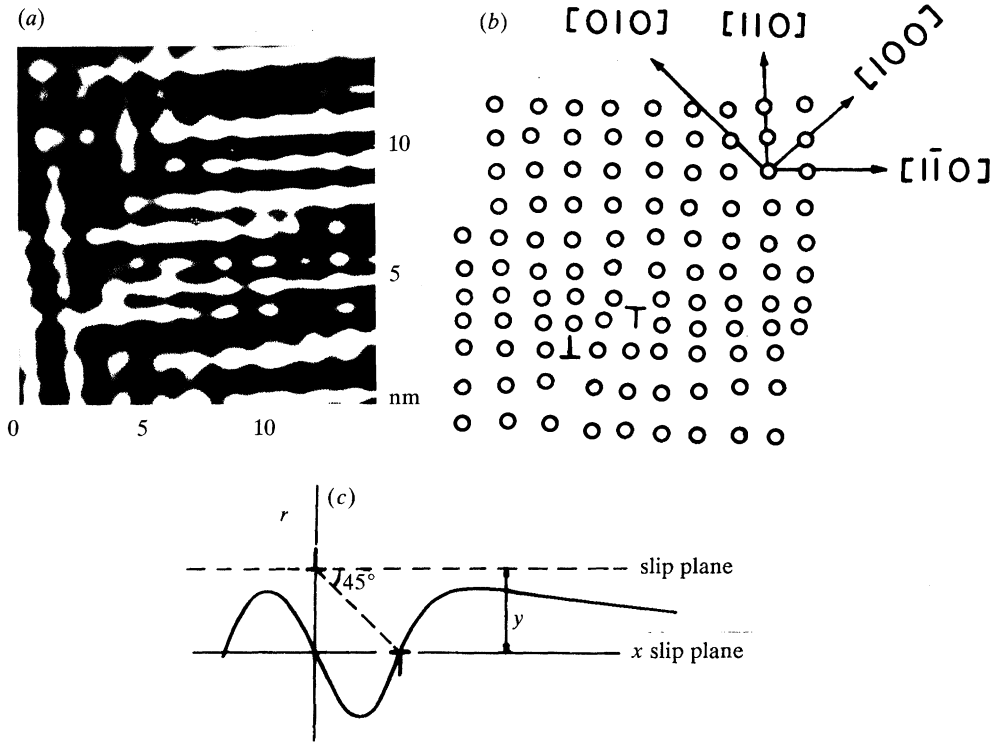

Figure 6. (*a*) Top view image of (001) plane over a scan area of 15×15 nm showing two unlike edge dislocations on the adjacent slip planes; their strain-fields tend to cancel each other as seen from the straightening-up of the lattice planes on from the straightening-up of the lattice planes on farther sides (bias voltage is -1955 mV, current is 50 pA, moderate filtering). (*b*) Sketch of figure 5*a*. The Burgers vector of the dislocation of figure 5*a* is $\pm\frac{1}{2}[1\bar{1}0] = \pm a/\sqrt{2}$. (*c*) Interaction between two unlike edge dislocations on neighbouring slip plane. The force is attractive and the stable equilibrium is attained for the 45° position shown which is corroborated with the image of figure 5*a* (for details see Cottrell 1953).

features more transparent to tunnelling. Also, with the present samples the images were obtained at a relatively higher bias voltage and extremely low tunnelling current of 50 pA. These conditions, we believe, were conducive for a better molecular imaging free from instability in our investigation.

Well resolved images of figures 3*a* and 4*a* depict a regular lattice free from any obvious imperfections. However, the sample did show regions containing lattice defects. This is illustrated in the top view image of figure 6*a* obtained over a scan area of 15×15 nm. As may be noticed from its sketch of figure 6*b*, the regular arrangement of (001) plane is disturbed by the presence of lattice defects. Two extra half-planes, characteristic of two edge dislocations of opposite sign are clearly visible. As their strain fields tend to cancel each other, the bent lattice planes in their immediate vicinity are gradually seen to get straightened as one moves away from them. From the crystallographic directions indicated in figure 6*b*, it is apparent that their Burgers vector $b = \pm\frac{1}{2}[1\bar{1}0] = \pm a/\sqrt{2}$, which is in conformity with the characteristic Burgers vector of a dislocation in the FCC lattice having $\langle 110 \rangle$ as the close packed direction for slip to occur. Since for a C_{60} solid, $a = 1.4$ nm, the magnitude of $b = 1.0$ nm. Incidently, this value is approximately three to four times larger than for the conventional metallic materials. Since the strain energy per unit

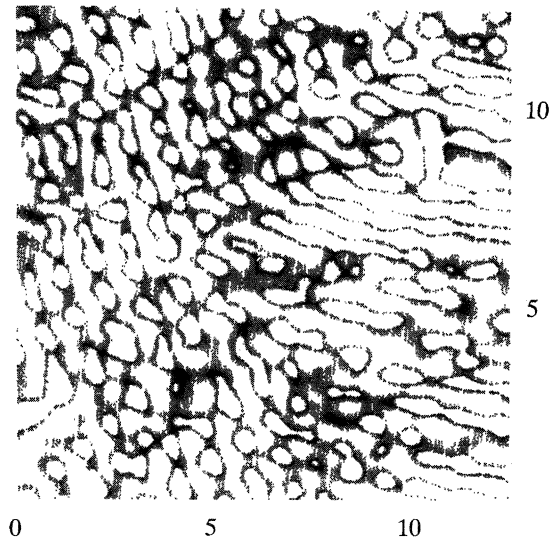

Figure 7. Top view image of (111) planes showing triangular arrangement of clusters with stacking disorders, zoomed over a scan area of 13 × 13 nm (bias voltage is −1401 mV and current is 50 pA; moderate filtering).

length of the dislocation is proportional to γb^2, where γ is the shear modulus, a dislocation would possess a greater line tension and as such we expect the dislocation lines in the C_{60} solid to be straight. It therefore seems unlikely that the two dislocations seen in figure 6 would be the entry and exit parts of one and the same dislocation loop of about 2 nm diameter. Large strain energy should make the dislocations in C_{60} solid more interactive. It is well established (Cottrell 1953) that the two unlike edge dislocations attract each other while the like ones repel, and the stable equilibrium position of the former on the parallel slip planes is at a 45° position, corresponding to $x = \pm y$ (figure 6*c*). Interestingly, the two dislocations of figure 6, observed on the adjacent parallel slip planes, are placed close to the 45° position, in accordance with the above contention. A mutual annihilation of these dislocations can occur only by climb which is a thermally activated process.

Since in FCC crystals, the most densely packed {111} planes undergo slip, we expect these planes to be most susceptable to defect formation. In contrast to figure 4*a*, showing a near ideal {111} configuration over a small area scan, the larger area scans obtained have revealed extensive defect structures in {111} planes, as depicted in figure 7. The figure is a top view scan over a size of 13 nm × 13 nm. A preliminary study of the relative heights of individual clusters located on equilateral triangles has suggested the possibility of a disorder in the neighbouring stacks of {111} planes in the *z*-direction resulting in the formation of surface defects such as twins and stacking faults, which need to be further studied. Incidently, the electron diffraction patterns (Grigoryan *et al.* 1992*b*) of the present series of samples have indicated the presence of twin boundaries corroborating the above observation.

In the above images, although the lattice structure of the C_{60} buckyballs is clearly observed, the submolecular features of the individual cages are not resolved. Using the imaging parameters as followed earlier (Narlikar *et al.* 1992) we could succeed in resolving the characteristic arrangement of hexagons and pentagons of an individual carbon cage. Two typical images obtained are shown in figure 8*a*, *b*, in 3D perspective

PHILOSOPHICAL TRANSACTIONS OF THE ROYAL SOCIETY A MATHEMATICAL, PHYSICAL & ENGINEERING SCIENCES

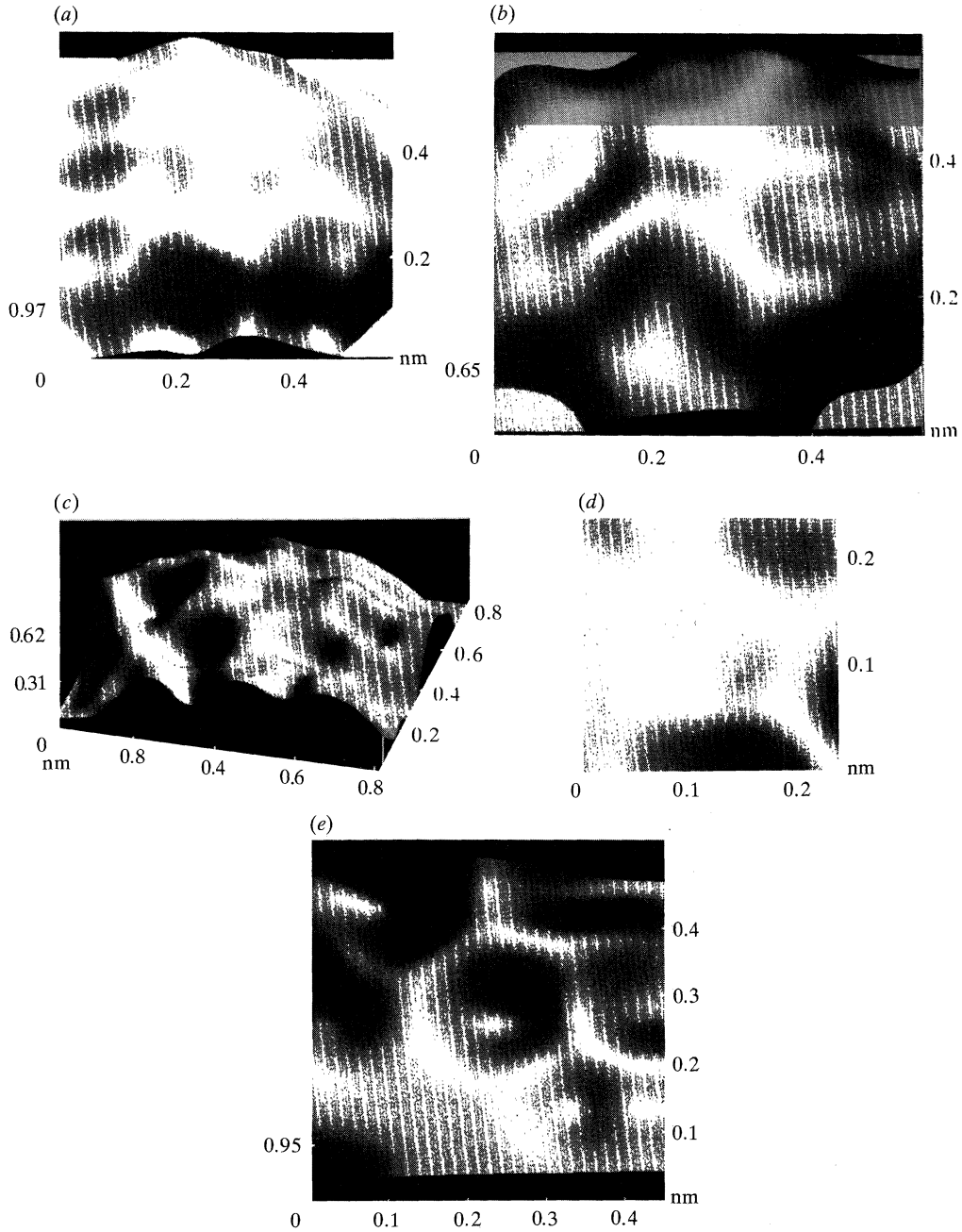

Figure 8. (*a*), (*b*) Typical images of two individual carbon cages in 3D perspective at 60° pitch, showing well-resolved pentagons and hexagons; (*c*) the carbon cage image in 3D perspective at 30° pitch; (*d*), (*e*) typical zoomed images of a pentagon and a hexagon (−550 mV, 50 pA, moderate filtering).

at 60° pitch. The image presented in figure 8*c* is in 3D perspective at 30° pitch. As may be seen, the pentagons and hexagons are found to follow the characteristic soccer ball pattern over the sphere of about 0.7 nm diameter. A typical pentagon and

Figure 9

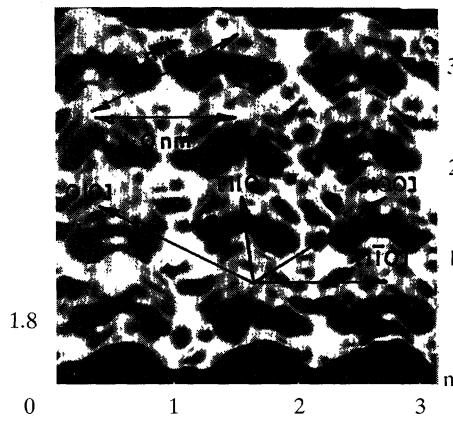

Figure 10

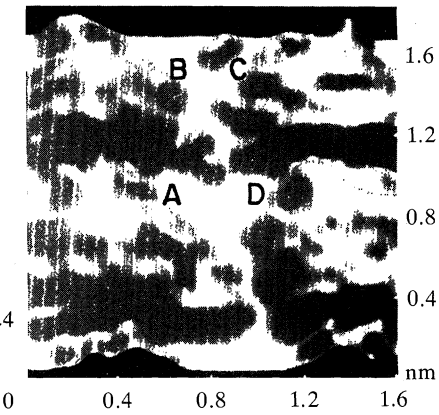

Figure 9. 3D perspective image in 60° pitch showing 12 bucky balls of 0.7 nm diameter with truncated icosahedral structure, over a scan area of about 3 nm × 3 nm filtering.

Figure 10. Zoomed image of four bucky balls from figure 9 (scan size: 1.6 nm × 1.6 nm), the two diagonally opposite balls A and C may be considered the corner sites while the other two, B and D as face centring ones of the neighbouring unit cells (or vice versa).

a hexagon are separately zoomed in figure 8*d* and *e* respectively. The bond lengths are in fair accord with the expected value of 0.14 nm (Raghavachari & Rohlfing 1991), though, presently, it has not been possible to differentiate between the single and double bond lengths.

Following the imaging procedure essentially as described earlier (Narlikar *et al.* 1992) we have attempted to see the relative orientations of the assemblage buckyballs located at corner and face-centring sites of the C_{60} lattice. The image thus obtained, showing 12 buckyballs in a scan area of *ca.* 3 nm × 3 nm, in 3D perspective at 60° pitch is presented in figure 9. Although, in respect of the cage structure the buckyball images of figure 9 are not sufficiently distinct, one can still note that they do seem to carry features which were absent in the previously presented lattice images. Four such balls have been zoomed in figure 10 which shows them in 3D perspective at 60° pitch. Clearly, there seems no orientational relationship between the features seen in the four carbon cage images, indicating a lack of any correlation between them. This is consistent with each molecule of the C_{60} solid, at ambient temperature, undergoing rotational diffusion which is uncorrelated with the motion of its neighbours and such an orientational disorder has presumably been retarded or frozen out in the present samples, leaving them in a random orientation with respect to each other.

One of the reasons for retardation or freezing of the rotational component has been ascribed in the beginning to the presence of higher fullerene derivatives in the samples. It was pointed out in our earlier communication (Narlikar *et al.* 1992) that in such samples exhibiting a reasonable conductivity the C_{60}–C_h interaction, may be dominating over the rotational interaction, which is of the order of 50 meV C^{-1} molecule (Tycko *et al.* 1991*b*) and be of the order of the band width of 0.1 eV. The micro-Raman studie of Grigoryan *et al.* (1992*a*) on the present series of samples do seem to give credence to the likely role of C_{60}–C_{70} interaction as suggested above and also corroborate the STS results as described earlier. This apart, as mentioned earlier, the present films had been deposited on silver electrodes over a glass surface, and as

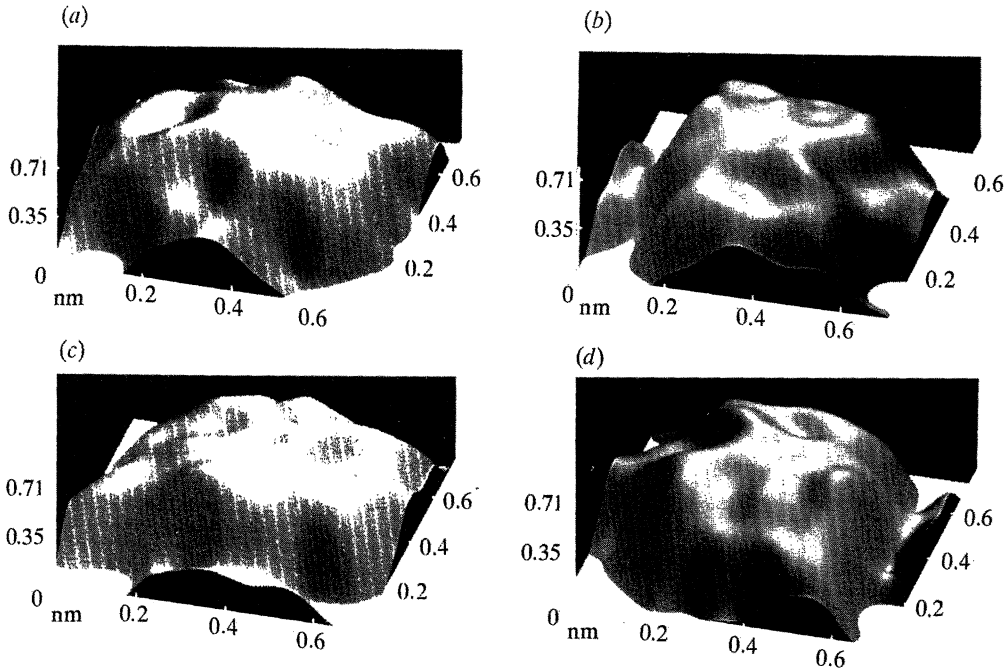

Figure 11. (*a*)–(*d*) 3D perspective image in 30° pitch of a single buckyball seen with successive 90° rotation showing distortions (scan size: 0.7 nm × 0.7 nm; bias voltage is −590 mV, current 50 pA, moderate filtering).

such the C_{60} molecules had silver atoms in their neighbourhood. Their interaction, as pointed out by Wilson *et al.* (1990) in case of C_{60} films on gold electrodes, can change the electronic structure of the films to make them conducting and simultaneously cause some retardation or freezing of the free rotation.

Another possible cause of the conducting nature of the present C_{60} films and of the rotational freezing of the molecules may be linked with the buckyball distortion. It is worth noting that, in general, we have found the STM images of the individual buckyballs to be somewhat distorted. The effect may be seen in figure 11*a*[d] depicting four images of the same buckyball, in 3D perspective at 30° pitch, as seen after successive 90° rotation. Clearly, the buckyball observed is not ideally spherical but appears to be asymmetric and distorted. As a result of asymmetry, the energy gap is expected to be reduced. As per theoretical calculations of Yi & Bernholc (1992) even small distortions in the carbon cage, such as resulting from the creation of two pentagon pairs, the HOMO–LUMO gap can be reduced by 0.6 eV mol^{-1}. Our recent STM studies (Dutta *et al.* 1993) have indeed detected such pentagon pairs in the present series of samples. The diminished energy gap due to buckyball distortions would promote a more effective hybridization and explain the conducting nature of the films, and at the same time would cause retardation or freezing of the rotational motion.

The problem of distortions of the carbon cage has emerged as an area of great topical interest for theoretical chemists (Yi & Bernholc 1992; Raghavachari & Rohlfing 1992; Chelikowsky 1991; Wang *et al.* 1992). The molecular dynamics simulations have been performed under varying constraints which have predicted, besides the pentagon pairs, a host of other defect structures, which include,

PHILOSOPHICAL TRANSACTIONS OF THE ROYAL SOCIETY A MATHEMATICAL, PHYSICAL & ENGINEERING SCIENCES

heptagons, octagons, puckerd hexagons, fused pentagons, etc., some of which we have been able to observe recently through STM and which form the subject matter of a separate communication, under preparation. These distortions may be intrinsically present during sample processing when, at high temperatures, the chain of carbon atoms are nucleated and during the subsequent cooling it takes the form of five- and six-member rings (Yi & Bernholc 1992; Raghavachari & Rohlfing 1992; Chelikowsky 1991; Wang *et al.* 1992). If the cooling is relatively fast, the metastable state, comprising of defects, may be frozen in. Alternatively, the distortions might result from the large electric field gradient present between the sample surface and the STM tip during tunnelling. Such field gradients are known to influence the molecular motion (Ohitani *et al.* 1988). A sufficiently large field gradient, may cause both the distortion of carbon cages and simultaneously inhibit the rotational diffusion. Clearly, this possibility may be checked using an AFM where there is no electric field present between the vibrating cantilever and the sample surface. In this connection, it is interesting to mention the recent AFM studies of Dietz *et al.* (1992), which also depict some distortions in the buckyball images. The nonlinearity effects in piezoelectric scanner have been suggested as the possible cause for distortions by the above authors. However, clearly, the precise explanation is to be investigated in terms of the defect structures of the distorted cage in the light of various theoretical models (Yi & Bernholc 1992; Raghavachari & Rohlfing 1992; Chelikowsky 1991; Wang *et al.* 1992) and the observational evidence yielded by both STM and AFM which is presently underway.

4. Summary

To sum up, the described STM studies of C_{60} films containing conducting islands have revealed the FCC lattice of the C_{60} clusters with intermolecular distances in various planes, along different directions, in close accord with the reported data based on XRD and neutron diffraction analysis. The molecular lattice is found to contain extended defects, crystallographically consistent with the FCC structure. The characteristic cage morphology of the buckyballs in the form of hexagons and pentagons has been resolved individually as well as in the lattice. The high resolution zoomed images of the latter corroborate X-ray and neutron diffraction data indicating that the orientational disorder has been frozen out from a state in which each C_{60} molecule of the FCC lattice is undergoing a rotational motion which is uncorrelated with the motion of its neighbours. The retardation or freezing of the rotational diffusion has been attributed to various reasons which include the large electric field effect between the sample surface and the STM tip. The latter could be one of the reasons of the distortions observed in the buckyball images which is being further investigated using AFM.

We thank Dr L. S. Grigoryan for providing the samples synthesized at the IIT (Kanpur). We also thank our colleague Dr Ratan Lal of the Theory Group for many stimulating discussions and we are indebted to Professor S. K. Joshi, Director General, CSIR for his continued interest. Some useful suggestions made by Professor Alan Mackay of the University of London and Professor M. V. Sadovskii of the Russian Academy of Sciences (Ural Branch) are acknowledged.

References

Bethune, D. S., Meijer, G., Tang, W. C. & Rosen, H. J. 1990 The vibrational Raman spectra of purified solid films of C_{60} and C_{70}. *Chem. Phys. Lett.* **174**, 219–222.

Chelikowsky, J. R. 1991 Nucleation of C_{60} clusters. *Phys. Rev. Lett.* **67**, 2970–2973.

Cottrell, A. H. 1953 *Dislocations and plastic flow in crystals*, pp. 45–51. Oxford: Clarendon Press.

David, W. I. F., Ibberson, R. M., Matthewman, J. C., Prassides, K., Denis, T. J. S., Hare, J. P., Kroto, H. W., Taylor, R. & Walton, D. R. M. 1991 Crystal structure and bonding of ordered C_{60}. *Nature, Lond.* **353**, 147–149.

Dietz, P., Fostiropoulos, K., Kratschmer, W. & Hansma, P. K. 1992 Size and packing of fullerenes on C_{60}/C_{70} crystal surfaces studied by atomic force microscopy. *Appl. Phys. Lett.* **60**, 62–64.

Douglas, B. E. & McDaniel, D. H. 1975 *Concept and model of inorganic chemistry*, p. 76. London: Blaisdell.

Dutta, P. K., Samanta, S. B. & Narlikar, A. V. 1993 Nanometric lattice defects and distortion in the buckyball cage in C_{60} films revealed by scanning tunnelling microscopy. *Phil Mag. Lett.* (In the press.)

Grigoryan, L. S., Bist, H. D., Clara, H., Sudhakar, N., Prem Chand, Majumdar, A. K., Dutta, P. K., Samanta, S. B. & Narlikar, A. V. 1992*a* Electron-molecular vibration interactions in undoped fullerene films: a micro-Raman study. *Chem. Phys. Lett.* **199**, 360–364.

Grigoryan, L. S., Prem Chand, Sharma, S. V. & Majumdar, A. K. 1992*b* Nanocluster composites: synthesis, characterization and expectations. *Sol. State Commun.* **81**, 853–857.

Grigoryan, L. S., Bist, H. D., Sathaiah, S., Sharma, S. V., Clara, H. & Majumdar, A. K. 1992*c* Micro-Raman spectroscopy of carbon cluster composites. *J. Raman Spectroscopy* **23**, 127–131.

Hawkins, J. M., Meyer, A., Lewes, T. A., Loren, S. & Hollander, F. J. 1991 Crystal structure of osmylated C_{60}: confirmation of soccerball framework. *Science, Wash.* **252**, 312–313.

Hebard, A. F., Rosseinsky, M. J., Haddon, R. C., Murphy, D. W., Glarum, S. H., Palstra, T. T. M., Ramirez, A. P. & Kortan, A. R. 1991 Superconductivity at 18K in potassium doped C_{60}. *Nature, Lond.* **350**, 600–601.

Heiney, P. A., Fischer, J. E., McGhie, A. R., Romanow, W. J., Denenstein, A. M., McCauley, Jr, J. P., Smith, A. B. & Cox, D. E. 1991 Orientational ordering transition in solid C_{60}. *Phys. Rev. Lett.* **66**, 2911–2914.

Kratschmer, W., Lamb, L. D., Fostiropoulos, K. & Huffman, D. R. 1990 Solid C_{60} – a new form of carbon. *Nature, Lond.* **347**, 354–358.

Kroto, H. W., Heath, J. R., O'Brien, S. C., Curl, R. F. & Smalley, R. E. 1985 C_{60}-buckminsterfullerene. *Nature, Lond.* **318**, 162–163.

Lamb, L. D., Huffman, D. R., Workman, R. K., Howells, S., Chen, T., Sarid, D. & Ziola, R. F. 1992 Extraction and STM imaging of spherical giant fullerenes. *Sciences, Wash.* **255**, 1413–1416.

Lang, H. P., Thommen-Geiser, V., Frommer, J., Zahab, A., Bernier, P. & Guntherodt, H. J. 1992 Scanning tunnelling microscopy study of C_{60} on polycrystalline platinum. *Erophys. Lett.* **18**, 29–32.

Maniwa, Y., Mizoguchi, K., Kume, K., Kikuchi, K., Ikemoto, I:, Suzuki, S. & Achiba, Y. 1991 NMR investigation on the CS and benzene grown C_{60} crystals. *Solid State Commun.* **80**, 609–612.

Narlikar, A. V., Samanta, S. B., Dutta, P. K., Grigoryan, L. G. & Majumdar, A. K. 1992 Direct observation of carbon cage C_{60} buckyballs by scanning tunnelling microscopy. *Phil. Mag. Lett.* **66**, 75–79.

Ohtani, H., Wilson, R. J., Chiang, S. & Mate, C. M. 1988 Scanning tunnelling microscopy observations of benzene molecules on the Rh (111)–(3 × 3) (C_6H_6–2CO) surface. *Phys. Rev. Lett.* **60**, 2398–2401.

Raghavachari, K. & Rohlfing, C. M. 1991 Structures and vibrational frequencies of C_{60}, C_{70} and C_{84}. *J. phys. Chem.* **95**, 5768–5773.

Raghavachari, K. & Rohlfing, C. M. 1992 Imperfect fullerene structures: isomers of C_{60}. *J. phys. Chem.* **96**, 2463–2466.

Suzuki, T., Li, Q., Khemani, K. C., Wudl, F. & Almarsson, O. 1991 Systematic inflation of buckminsterfullerene C_{60}: synthesis of diphenyl fulleroids C_{61} to C_{66}. *Science, Wash.* **254**, 1186–1188.

Tycko, R., Haddon, R. C., Dabbagh, G., Glarum, S. H., Douglass, D. C. & Mujsce, A. M. 1991*a* Solid state magnetic resonance spectroscopy of fullerenes. *J. phys. Chem.* **95**, 518–520.

PHILOSOPHICAL TRANSACTIONS OF THE ROYAL SOCIETY A MATHEMATICAL, PHYSICAL & ENGINEERING SCIENCES

Tycko, R., Dabbagh, G., Fleming, R. M., Haddon, R. C., Makhija, A. V. & Zahurk, S. M. 1991*b* Molecular dynamics and phase transition in solid C_{60}. *Phys. Rev. Lett.* **67**, 1886–1889.

Vaughan, G. M., *et al.* 1992 Orientational disorder in solvent-free solid C_{60}. *Science, Wash.* **254**, 1350–1353.

Wang, C. Z., Xu, C. H., Chen, C. T. & Ho, M. 1992 Disintegration and formation of C_{60}. *J. phys. Chem.* **96**, 3563–3565.

Wilson, R. J., Meijer, G., Bethune, D. S., Johnson, R. D. Chambliss, D. D., de Vries, M. S., Hunziker, H. E. & Wendt, H. R. 1990 Imaging C_{60} clusters on a surface using a scanning tunnelling microscope. *Nature, Lond.* **348**, 621–622.

Wragg, J. L., Chamberlain, J. E., White, H. W., Kratischmer, W. & Huffman, D. R. 1990 Scanning tunnelling microscopy of solid C_{60} and C_{70}. *Nature, Lond.* **348**, 623–624.

Yi, J. Y. & Bernholc, J. 1992 Isomerization of C_{60} fullerenes. *J. chem. Phys.* **96**, 8634–8636.

Received 13 April 1992; accepted 5 February 1993

PHILOSOPHICAL TRANSACTIONS OF THE ROYAL SOCIETY A MATHEMATICAL, PHYSICAL & ENGINEERING SCIENCES

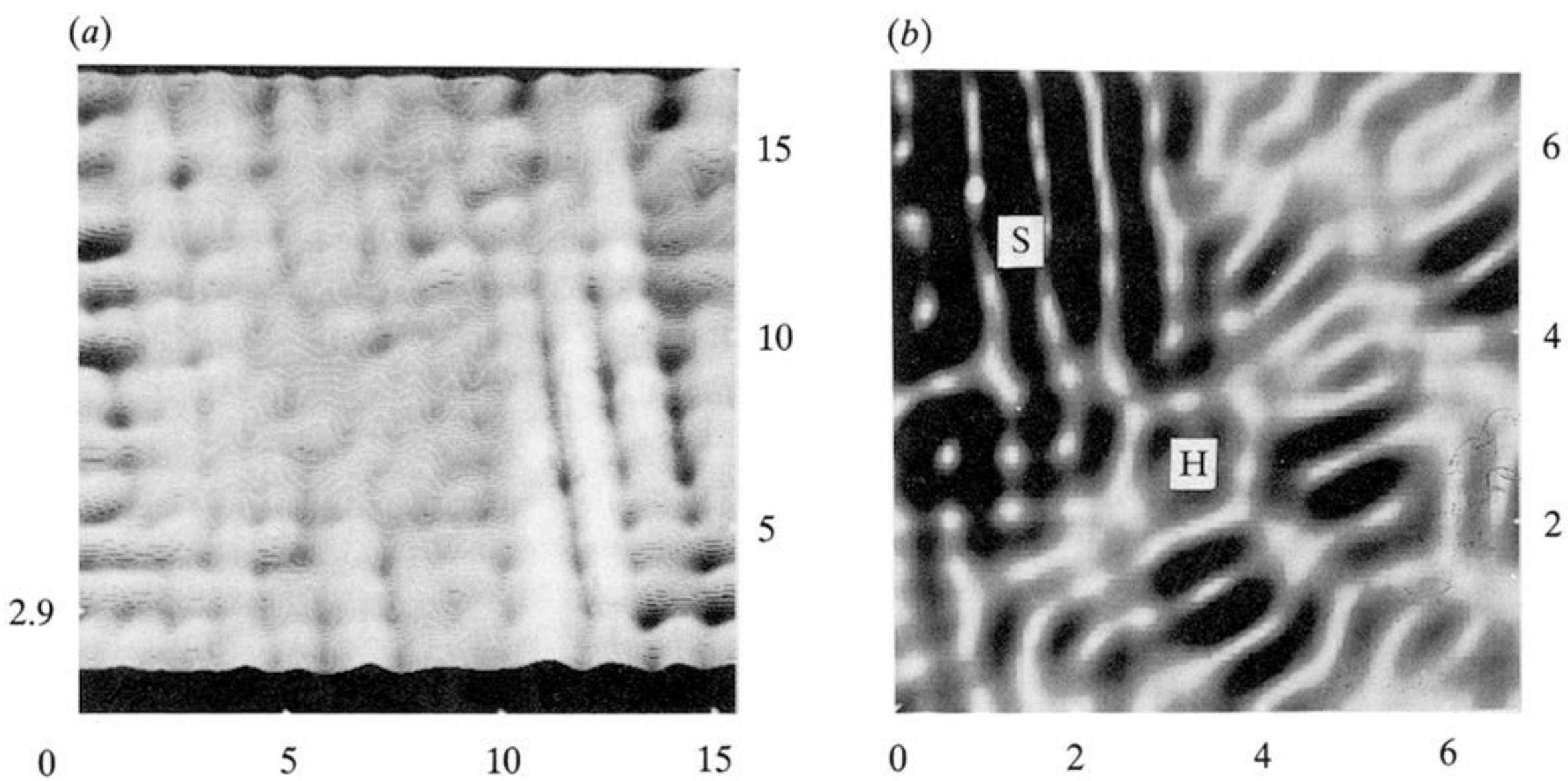

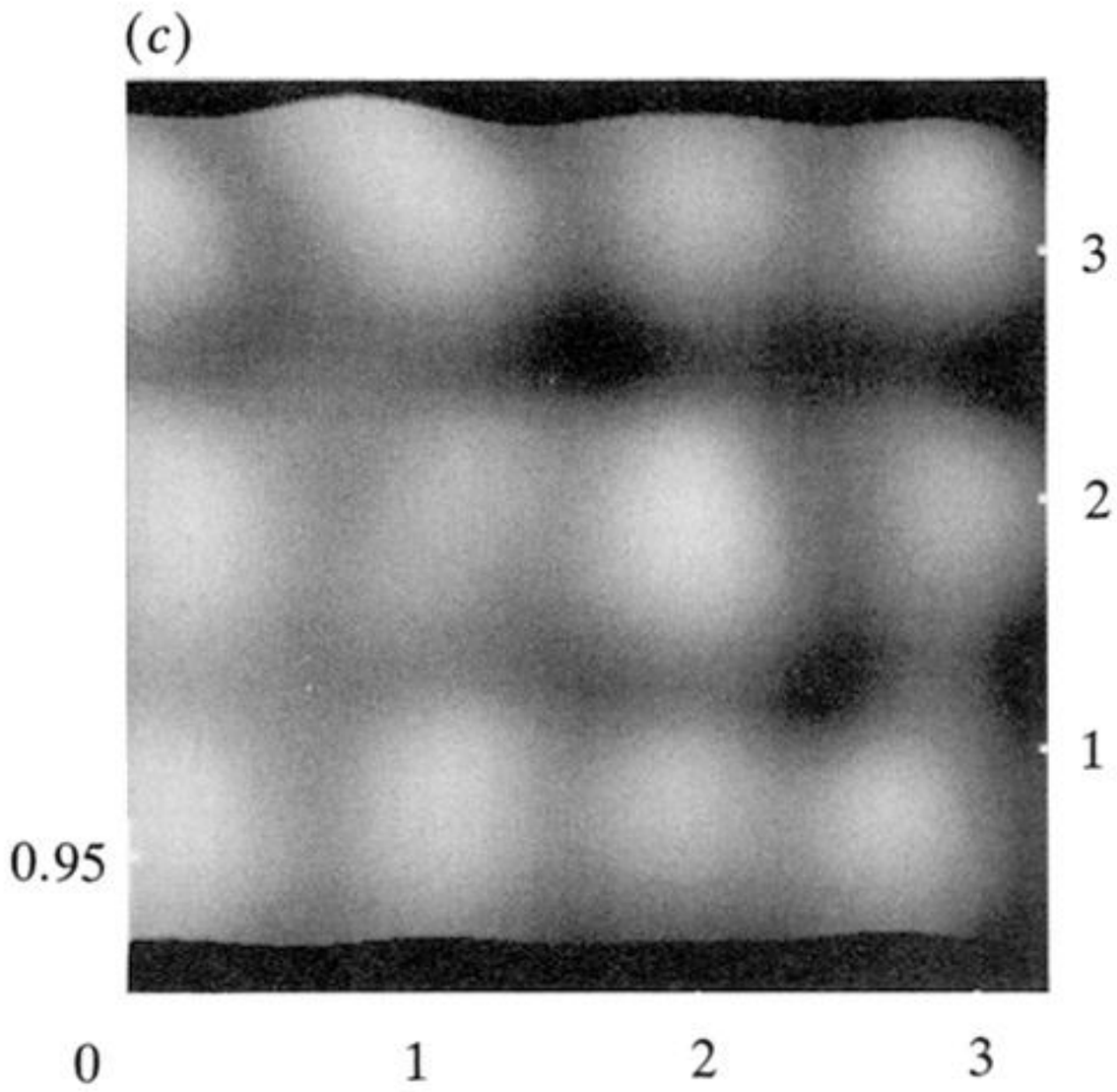

Figure 1. (*a*) Lattice-resolved CCs image in 3D perspective at 60° pitch over a scan area of 5×15 nm (bias voltage is 2400 mV and current is 50 pA; unfiltered), showing a square lattice arrangement at the outer periphery and unresolved pattern at the centre. (*b*) Zoomed image (scan size: 7×7 nm) of (*a*) covering parts the square lattice and unresolved patterns of (*a*), in the top view illumination mode revealing the unresolved pattern to be hexagonal (H) along with the square (S) lattice pattern. (*c*) Zoomed image (scan size: 3.2×3.2 nm; bias voltage is -2885 mV and current is 50 pA; moderately filtered) showing both smaller and larger size CCs on face corners and face centres of the FCC lattice.

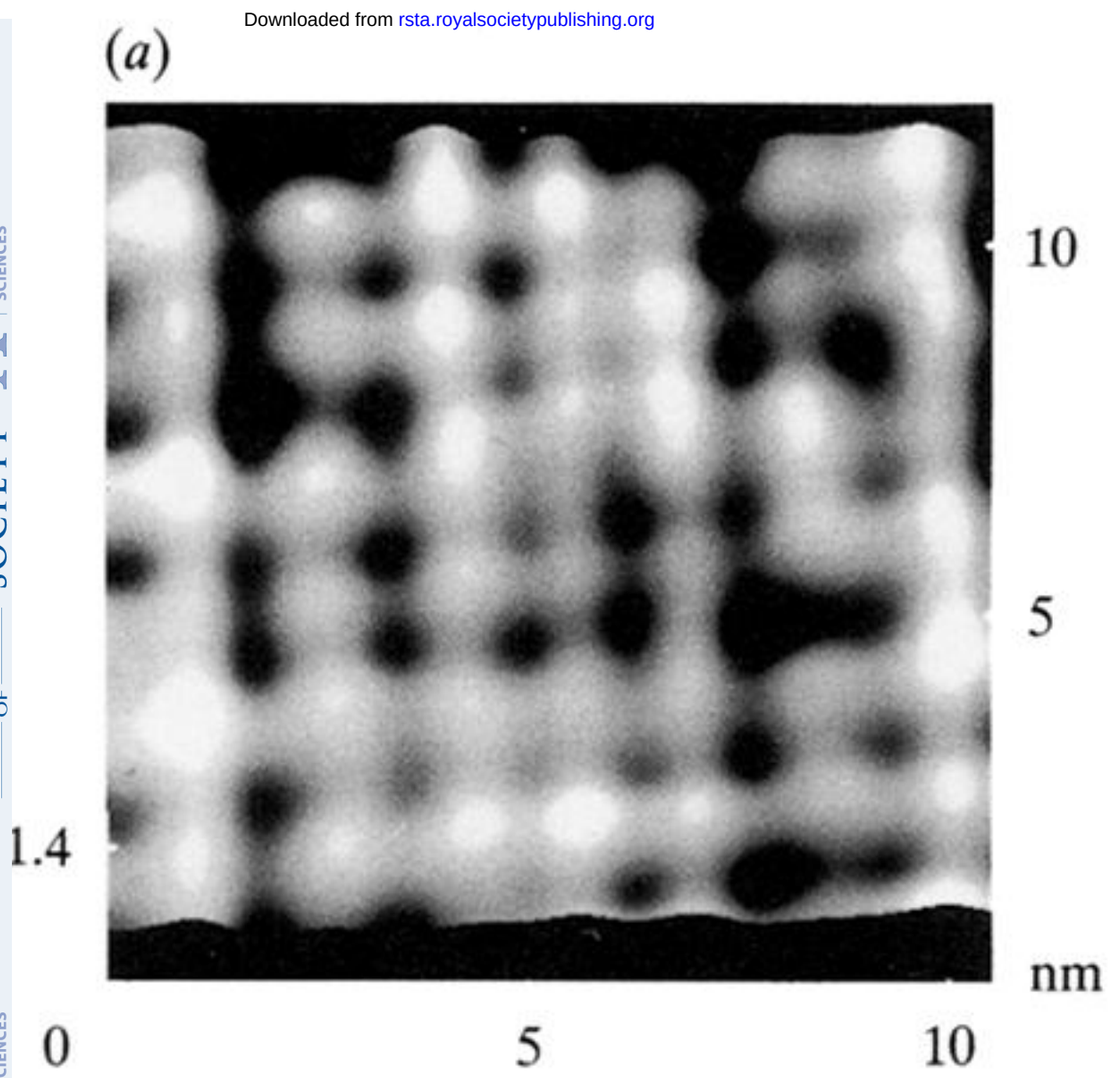

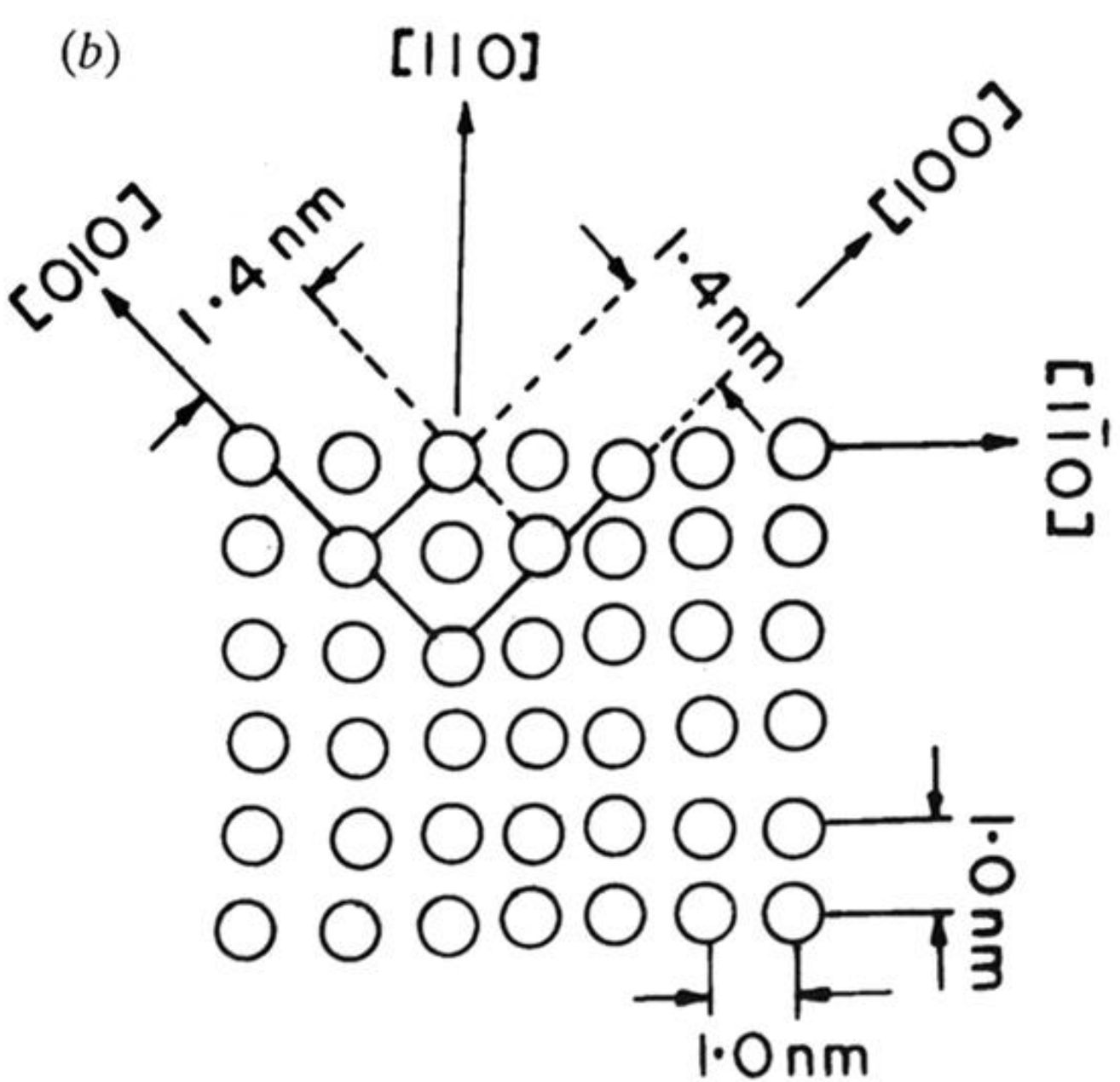

Figure 3. (*a*) Typical square lattice arrangement of CCs with no obvious lattice defects on a scan size: 10 × 10 nm; 3D perspective image in 60° pitch (bias voltage is −1955 mV, current is 50 pA, moderate filtering). (*b*) The sketch of the resolved pattern of (*a*) showing a square lattice pattern and the top view of FCC unit cell (001) plane. The prominent directions and intercluster distances indicated.

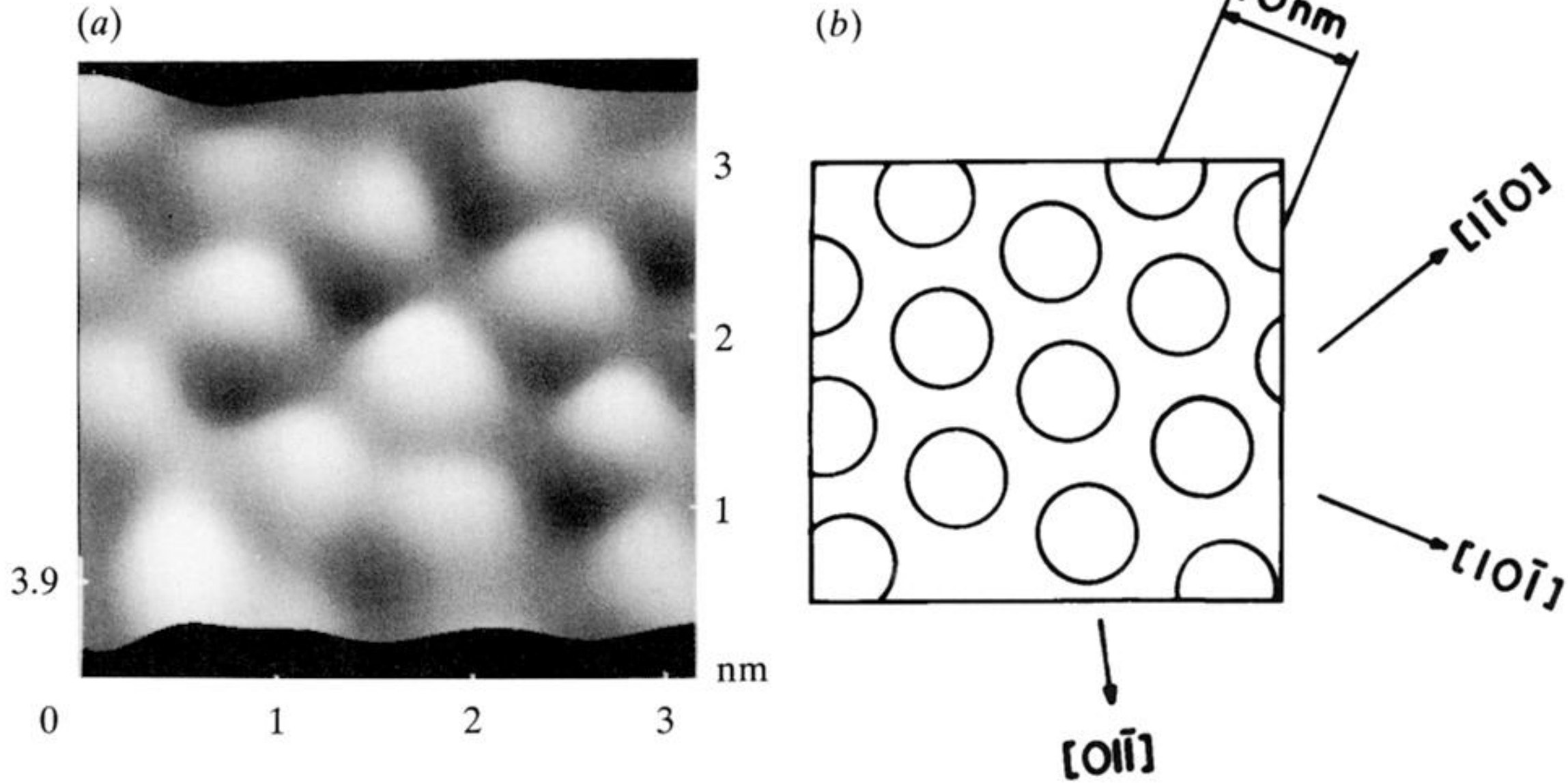

igure 4. (*a*) Typical triangular lattice arrangement of densely packed (111) planes of FCC structure n the zoomed image over a scan area of about 3.2×3.2 nm, in 3D perspective at 60° pitch (bias oltage is -1400 mV, current is 50 pA). The diameter of the balls is 0.7 nm. (*b*) The sketch of the esolved pattern of figure 3*b* with prominent directions and distances in (111) plane indicated.

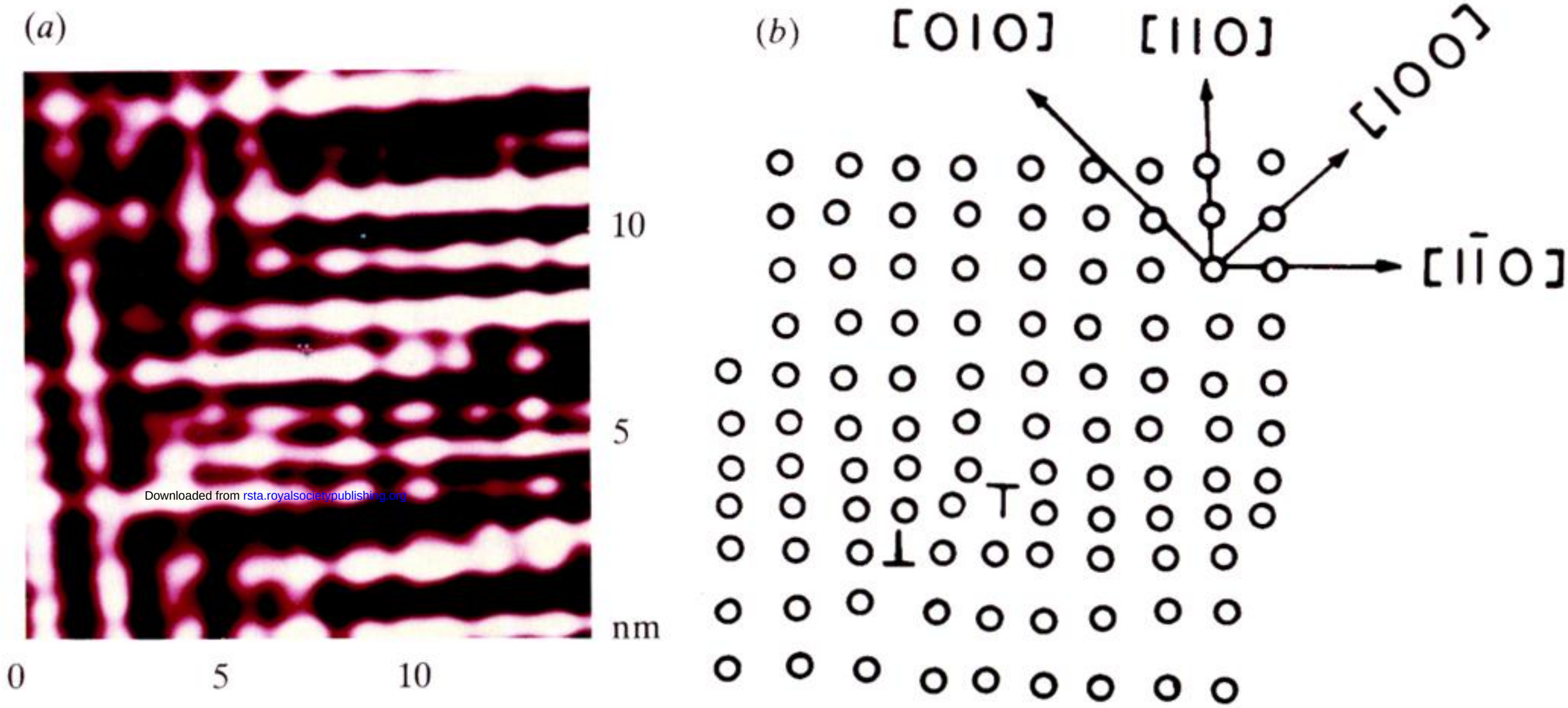

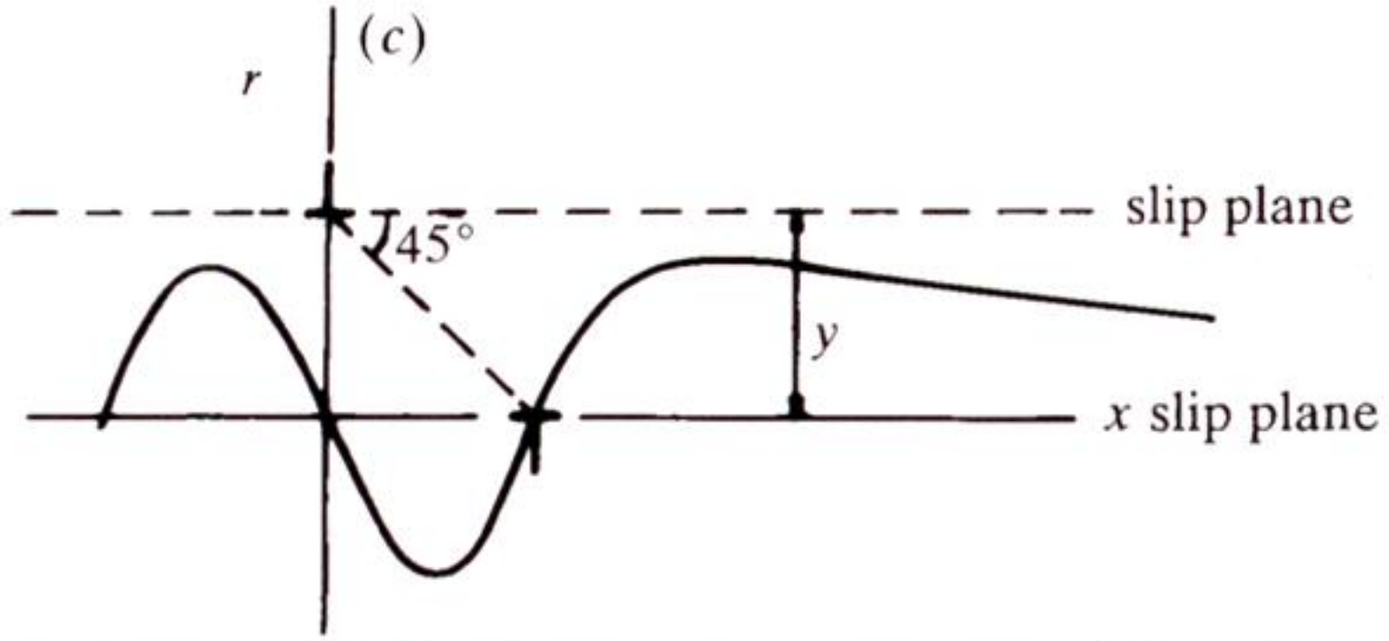

Figure 6. (*a*) Top view image of (001) plane over a scan area of 15×15 nm showing two unlike edge dislocations on the adjacent slip planes; their strain-fields tend to cancel each other as seen from the straightening-up of the lattice planes on from the straightening-up of the lattice planes on further sides (bias voltage is -1955 mV, current is 50 pA, moderate filtering). (*b*) Sketch of figure 6*a*. The Burgers vector of the dislocation of figure 5*a* is $\pm\frac{1}{2}[1\bar{1}0] = \pm a/\sqrt{2}$. (*c*) Interaction between two unlike edge dislocations on neighbouring slip plane. The force is attractive and the stable equilibrium is attained for the 45° position shown which is corroborated with the image of figure 6*a* (for details see Cottrell 1953).

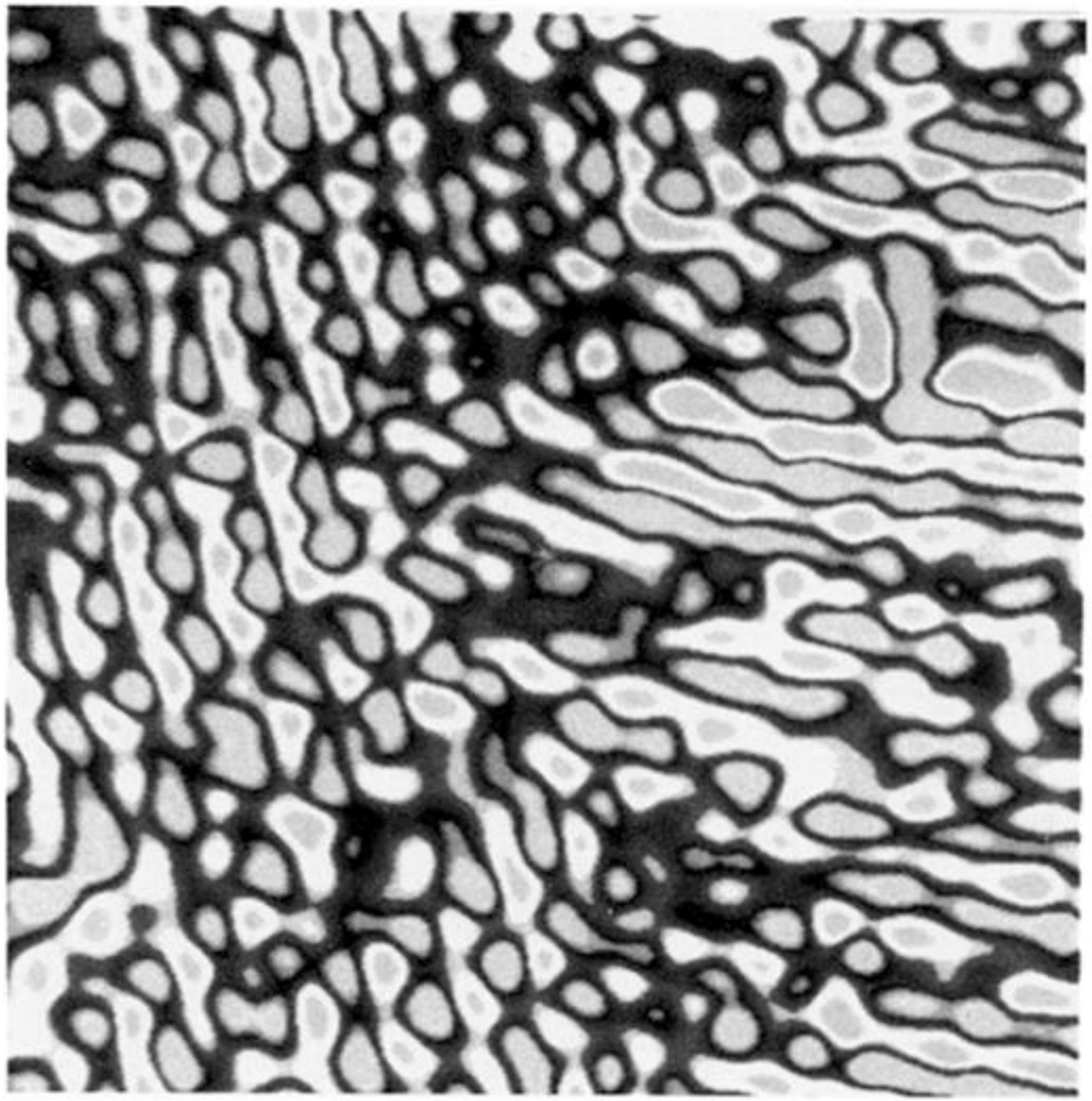

igure 7. Top view image of (111) planes showing triangular arrangement of clusters with stacking sorders, zoomed over a scan area of 13 × 13 nm (bias voltage is −1401 mV and current is 50 pA; oderate filtering).

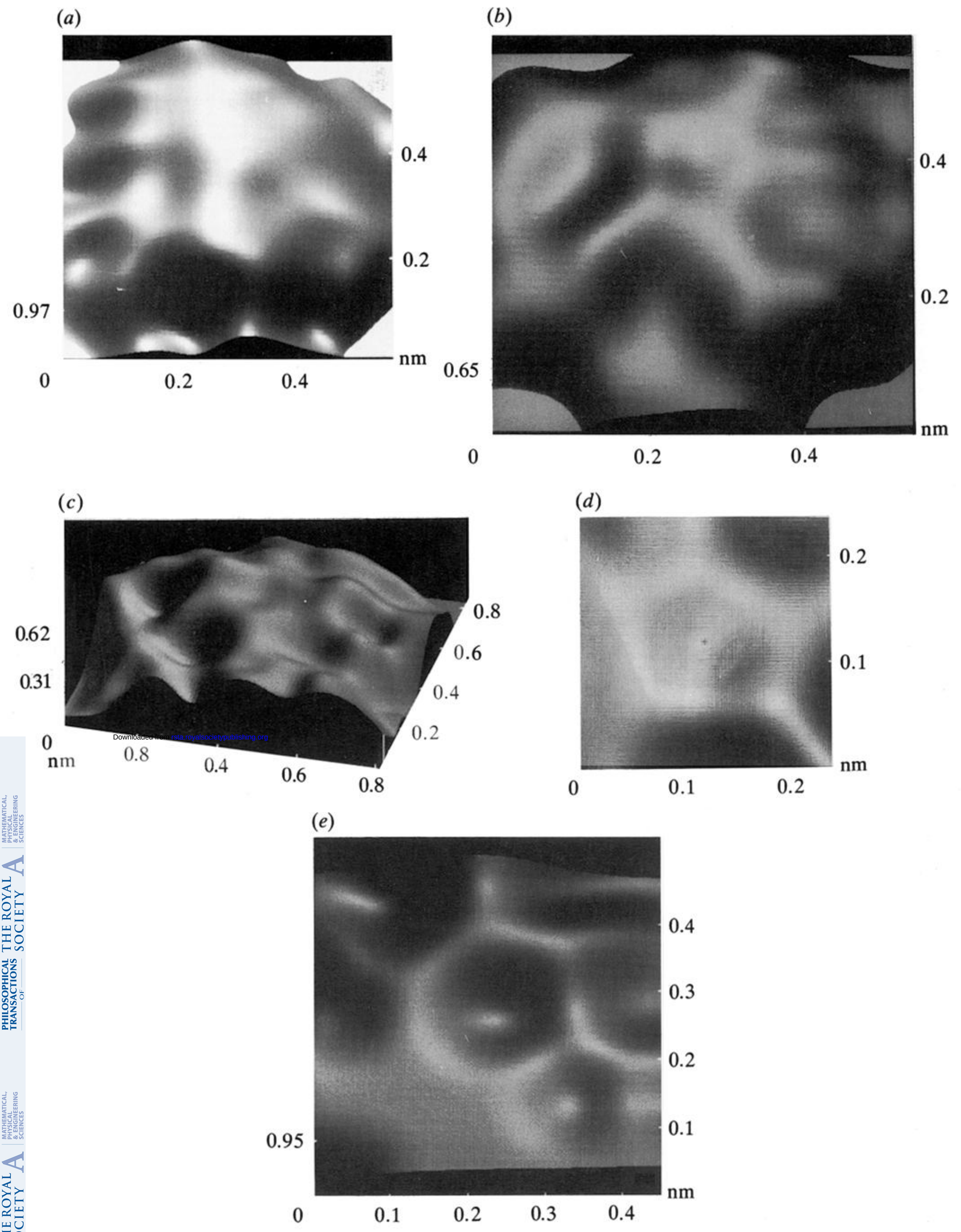

igure 8. (*a*), (*b*) Typical images of two individual carbon cages in 3D perspective at 60° pitch, owing well-resolved pentagons and hexagons; (*c*) the carbon cage image in 3D perspective at 30° tch; (*d*), (*e*) typical zoomed images of a pentagon and a hexagon (−550 mV, 50 pA, moderate tering).

Figure 9

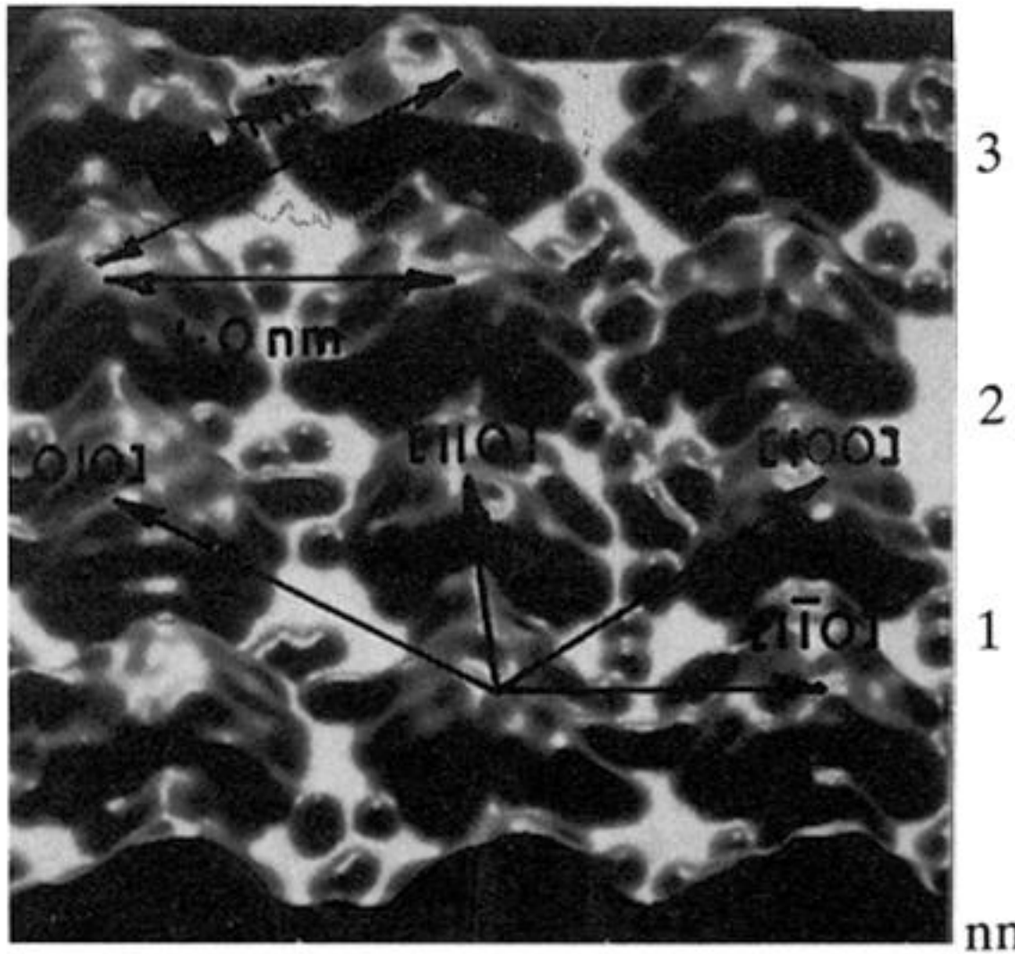

Figure 10

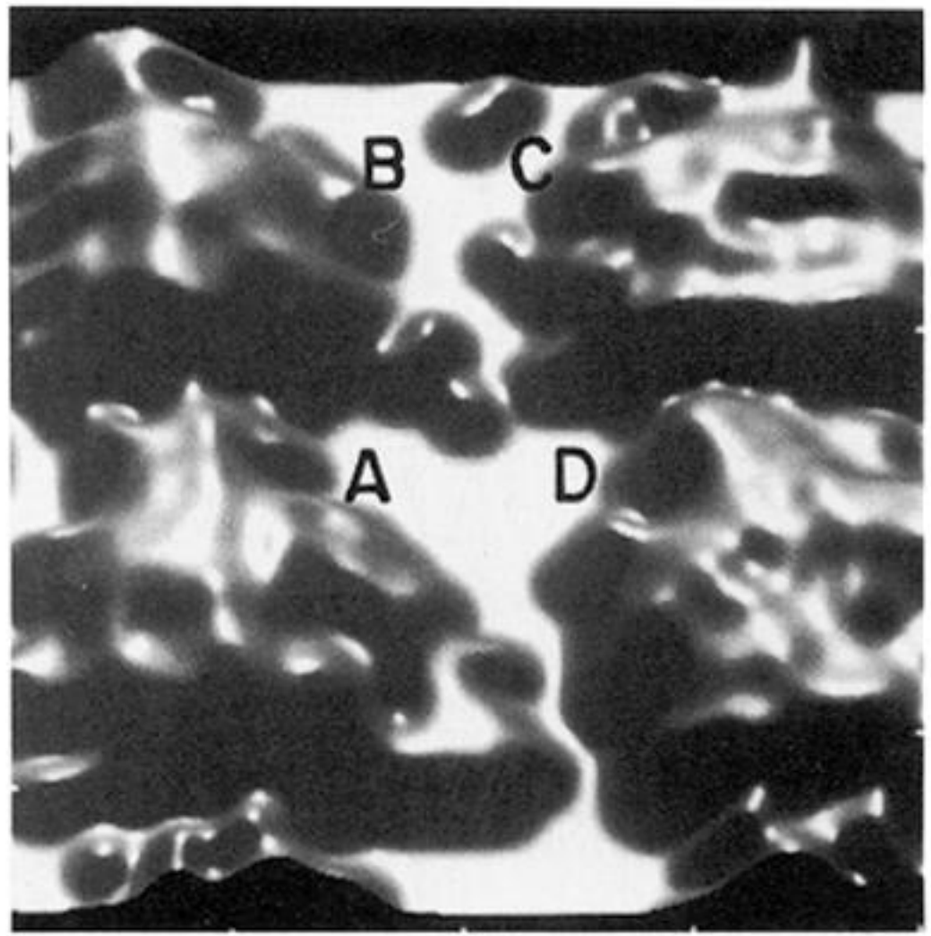

igure 9. 3D perspective image in 60° pitch showing 12 bucky balls of 0.7 nm diameter with uncated icosahedral structure, over a scan area of about 3 nm × 3 nm filtering.

igure 10. Zoomed image of four bucky balls from figure 9 (scan size: 1.6 nm × 1.6 nm), the two agonally opposite balls A and C may be considered the corner sites while the other two, B and as face centring ones of the neighbouring unit cells (or vice versa).

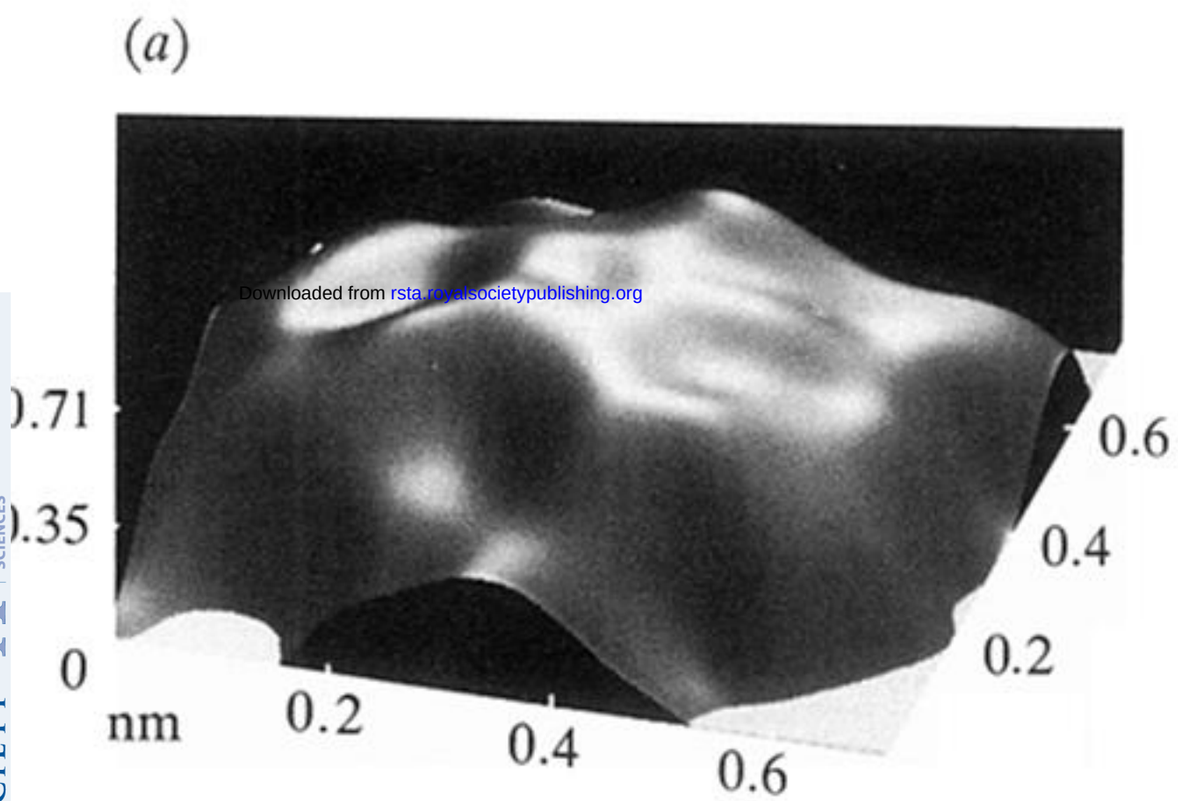

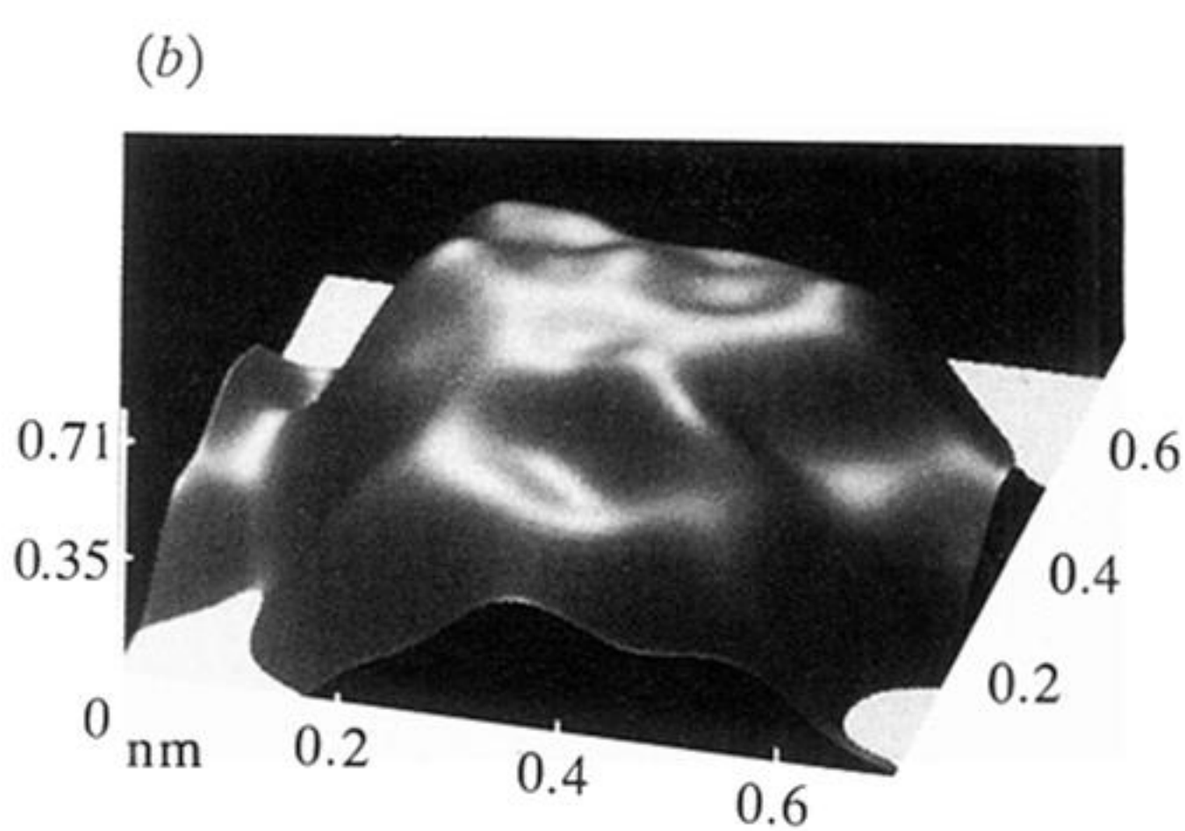

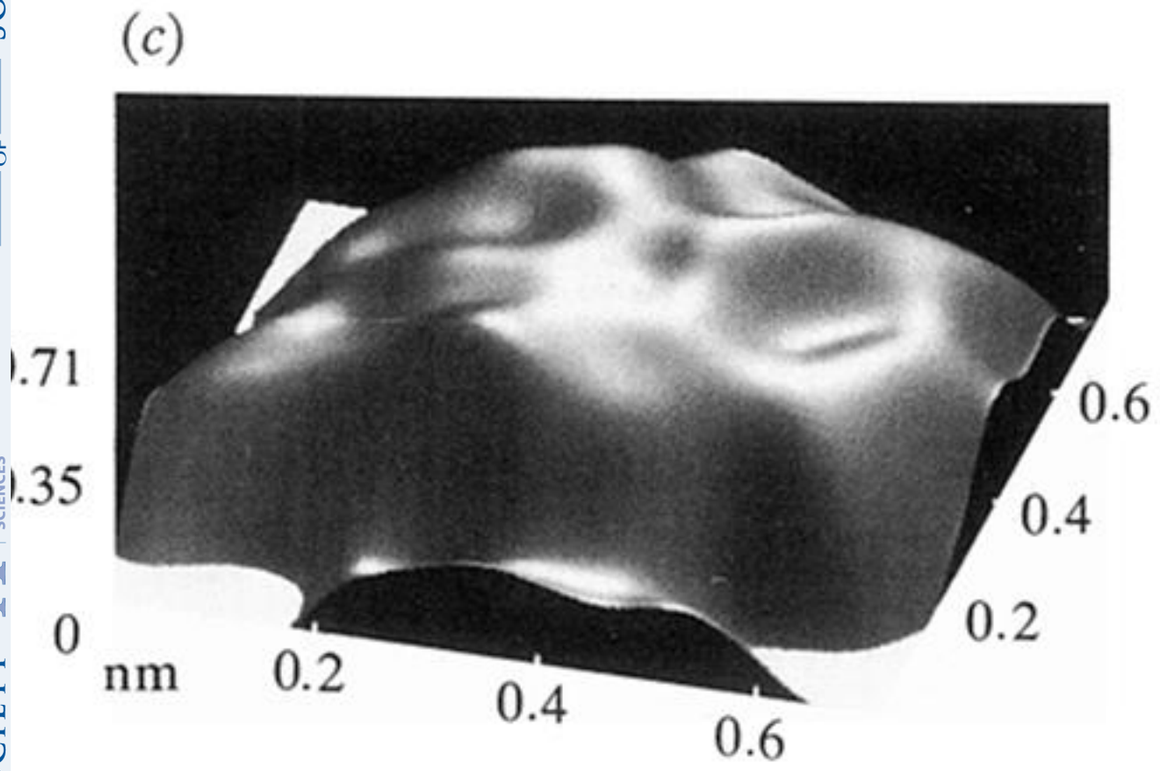

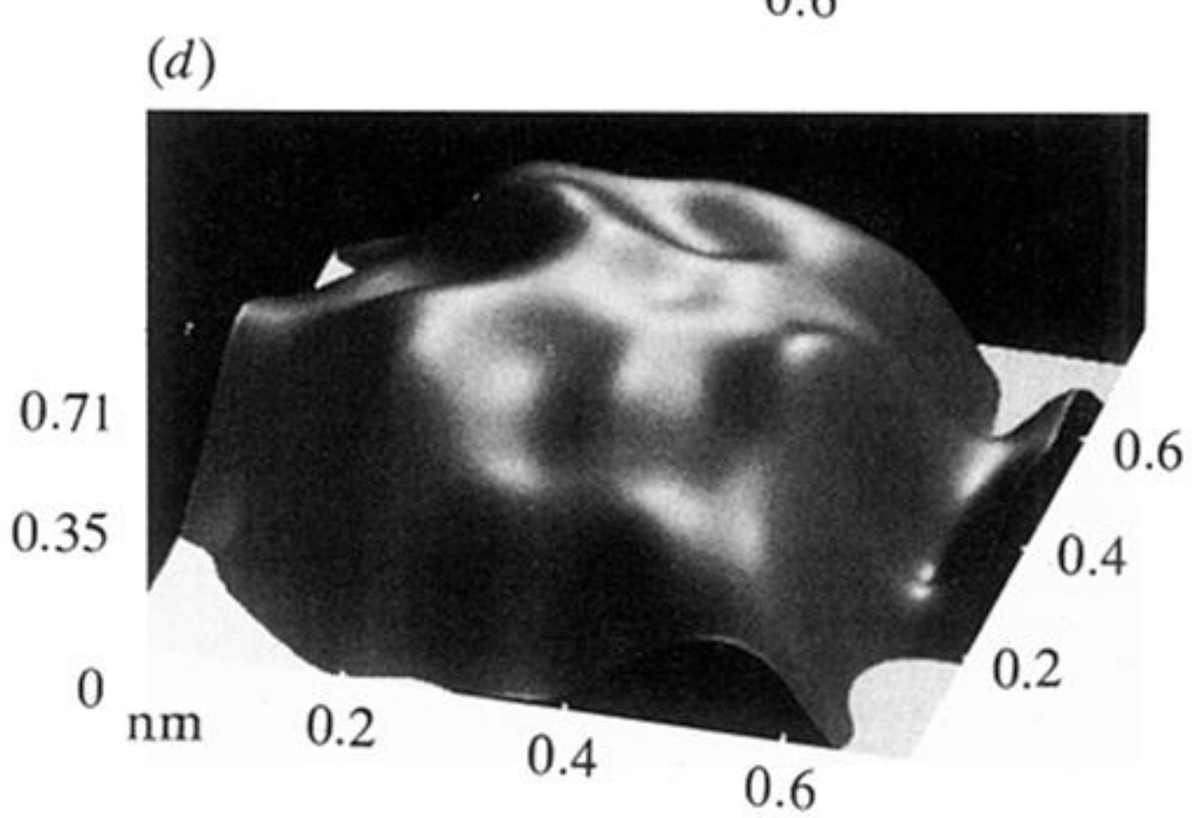

Figure 11. (*a*)–(*d*) 3D perspective image in 30° pitch of a single buckyball seen with successive 90° rotation showing distortions (scan size: 0.7 nm × 0.7 nm; bias voltage is −590 mV, current 50 pA, moderate filtering).